







Interaction with the CCT chaperonin complex limits APOBEC3A cytidine deaminase cytotoxicity

Abby M Green^{1,2,*} , Rachel A DeWeerd¹ , David R O'Leary¹ , Ava R Hansen¹ ,
Katharina E Hayer^{3,4} , Katarzyna Kulej³, Ariel S Dineen³, Julia H Szeto³, Benjamin A Garcia^{5,6} &
Matthew D Weitzman^{3,6,7,**} 

Abstract

The APOBEC3 cytidine deaminases are implicated as the cause of a prevalent somatic mutation pattern found in cancer genomes. The APOBEC3 enzymes act as viral restriction factors by mutating viral genomes. Mutation of the cellular genome is presumed to be an off-target activity of the enzymes, although the regulatory measures for APOBEC3 expression and activity remain undefined. It is therefore difficult to predict circumstances that enable APOBEC3 interaction with cellular DNA that leads to mutagenesis. The APOBEC3A (A3A) enzyme is the most potent deaminase of the family. Using proteomics, we evaluate protein interactors of A3A to identify potential regulators. We find that A3A interacts with the chaperonin-containing TCP-1 (CCT) complex, a cellular machine that assists in protein folding and function. Importantly, depletion of CCT results in A3A-induced DNA damage and cytotoxicity. Evaluation of cancer genomes demonstrates an enrichment of A3A mutational signatures in cancers with silencing mutations in CCT subunit genes. Together, these data suggest that the CCT complex interacts with A3A, and that disruption of CCT function results in increased A3A mutational activity.

Keywords APOBEC3A; CCT chaperonin; cytidine deaminase; protein interaction; mutational signatures

Subject Categories Cancer; DNA Replication, Recombination & Repair; Post-translational Modifications & Proteolysis

DOI 10.15252/embr.202052145 | Received 22 November 2020 | Revised 2 July 2021 | Accepted 5 July 2021

EMBO Reports (2021) e52145

Introduction

The human genome encodes seven APOBEC3 cytidine deaminase enzymes that catalyze the conversion of cytidine bases to uracil on

single-stranded DNA substrates (Jarmuz *et al*, 2002; Yu *et al*, 2004; Byeon *et al*, 2013; Mitra *et al*, 2014). Subsequent processing of uracil leads to mutations and DNA breaks. Several of the human APOBEC3 enzymes (named A3A through A3H) have the capacity to act as anti-viral effectors through deamination of viral genomes, resulting in widespread mutations, genome degradation, and restriction of infectivity (Chen *et al*, 2006; Vartanian *et al*, 2008; Malim & Bieniasz, 2012; Ooms *et al*, 2012; Harris & Dudley, 2015). However, in what is presumed to be off-target activity, APOBEC3 enzymes can also access and deaminate the cellular genome (Landry *et al*, 2011; Suspene *et al*, 2011; Burns *et al*, 2013a; Green *et al*, 2016). Two of the APOBEC3 family members, A3A and A3B, have been implicated as sources of mutagenesis in human cancers (Nik-Zainal *et al*, 2012; Alexandrov *et al*, 2013; Burns *et al*, 2013a; Alexandrov *et al*, 2016; Petljak *et al*, 2019). Elevated expression of APOBEC3 enzymes, along with mutational patterns consistent with cytidine deaminase activity, have been identified in tumors (Burns *et al*, 2013a; Roberts *et al*, 2013; Petljak & Alexandrov, 2016; Cancer Genome Atlas Research Network *et al*, 2017; Green *et al*, 2017; Cortez *et al*, 2019; Jalili *et al*, 2020). These observations suggest that aberrant activity of APOBEC3 enzymes may contribute to oncogenesis, clonal diversity, tumor evolution, and chemotherapy resistance (Burns *et al*, 2013a; Roberts *et al*, 2013; Faltas *et al*, 2016; Roper *et al*, 2019).

The concept of off-target APOBEC3 activity is ill-defined, since the regulation of APOBEC3 expression and activity under non-pathogenic conditions remains enigmatic. Basal expression levels of APOBEC3 enzymes are low in most healthy tissues (Koning *et al*, 2009; Refsland *et al*, 2010). Expression of two APOBEC3 family members, A3A and A3G, is upregulated by type I interferon stimulation of hematopoietic cells and keratinocytes (Chen *et al*, 2006; Koning *et al*, 2009; Wang *et al*, 2014), likely reflecting an innate immune response to viral pathogens (Peng *et al*, 2006; Mohanram *et al*, 2013). However, regulatory measures that ensure the host genome is protected from APOBEC3 activity have not been

¹ Department of Pediatrics, Washington University School of Medicine, St. Louis, MO, USA

² Department of Pathology and Immunology, Washington University School of Medicine, St. Louis, MO, USA

³ Department of Pathology and Laboratory Medicine, Children's Hospital of Philadelphia and University of Pennsylvania Perelman School of Medicine, Philadelphia, PA, USA

⁴ Department of Biomedical and Health Informatics, Children's Hospital of Philadelphia, Philadelphia, PA, USA

⁵ Department of Biochemistry and Biophysics, Perelman School of Medicine, University of Pennsylvania, Philadelphia, PA, USA

⁶ Perelman School of Medicine, Epigenetics Institute, University of Pennsylvania, Philadelphia, PA, USA

⁷ Center for Childhood Cancer Research, Children's Hospital of Philadelphia, Philadelphia, PA, USA

*Corresponding author. Tel: +1 314 273 3935; e-mail: abby.green@wustl.edu

**Corresponding author. Tel: +1 267 425 2068; e-mail: weitzmanm@email.chop.edu

elucidated. Given the proposed role of APOBEC3 enzymes in cancer mutagenesis, we sought to identify APOBEC3 protein binding partners in order to determine potential regulators of host genome deamination. Here, we show that A3A interacts with and is regulated by the chaperonin-containing TCP-1, CCT (also called TRiC) complex.

The CCT complex is a molecular chaperonin that enables folding of newly translated proteins to promote physiologic localization and activity (Yam *et al*, 2008; Joachimiak *et al*, 2014; Lopez *et al*, 2015). CCT is a double-ring oligomer comprised of eight subunits which encompass client proteins in an ATP-dependent manner (Booth *et al*, 2008; Cong *et al*, 2012; Reissmann *et al*, 2012). The canonical roles of this complex include folding of nascent proteins and prevention of protein aggregation (Thulasiraman *et al*, 1999; Kitamura *et al*, 2006; Tam *et al*, 2006; Yam *et al*, 2008). The CCT complex interacts with ~15% of newly synthesized proteins (Yam *et al*, 2008), and although the fraction that require CCT for folding and proper function is likely smaller, CCT plays an important role in essential cellular processes through protein homeostasis (Tyedmers *et al*, 2010; Hartl *et al*, 2011; Lopez *et al*, 2015). Notable clients of the CCT complex include cytoskeletal components actin and tubulin, oncoproteins TP53, von Hippel–Lindau, and STAT3, and checkpoint complex proteins PLK1 and CDC20 (Gao *et al*, 1992; Gao *et al*, 1993; Rommelaere *et al*, 1993; Feldman *et al*, 1999; Camasses *et al*, 2003; Liu *et al*, 2005; Trinidad *et al*, 2013; Kasembeli *et al*, 2014; Kaisari *et al*, 2017). Experimental deficiency of the CCT complex has resulted in phenotypes ranging from cancer to neurologic disorders, highlighting its broad role in cellular function (Jin *et al*, 2019).

In this study, we investigated protein interactors of A3A using affinity purification and mass spectrometry (MS). Surprisingly, we identified all eight subunits of the CCT complex by MS upon immunoprecipitation of A3A. Our MS findings were validated across a panel of cell lines by co-precipitation of A3A and the CCT complex. Furthermore, we demonstrated that depletion of the CCT complex results in increased DNA damage and cytotoxicity caused by A3A. Through *in silico* evaluation of cancer genome sequences, we found that A3A mutational signatures are enriched in tumors with CCT gene mutations. Together, our data point to the CCT chaperonin as a regulator of A3A that mitigates off-target deamination of the genome.

Results and Discussion

APOBEC3A interacts with the CCT molecular chaperonin complex

To identify protein interactors of A3A, we developed a U2OS-HiLo cell line with doxycycline-inducible HA-tagged APOBEC3A. The HiLo system enables recombination-mediated genomic integration of a single transgene per cell, leading to uniform expression levels of inducible genes in each cell (Khandelia *et al*, 2011). Inducible A3A expression in U2OS-HiLo cells was evaluated based on dose and duration of doxycycline treatment; a dose of 1 $\mu\text{g}/\text{ml}$ for 72 h was selected for immunoprecipitation experiments (Fig EV1A). There is significant variability in subcellular localization among APOBEC3 family members: three are expressed in the cytoplasm (A3F, A3G, A3H) and one is nuclear (A3B) (Lackey *et al*, 2012; Lackey *et al*, 2013). Unlike other APOBEC3 enzymes, A3A exhibits

pan-cellular localization (Landry *et al*, 2011; Lackey *et al*, 2013). Consistent with previous evaluations, A3A was detected in both nucleus and cytoplasm when induced in U2OS-HiLo cells (Fig EV1B). Anti-HA antibody was used to immunoprecipitate A3A-HA from U2OS-A3A cell lysates (Figs 1A and EV1C). Doxycycline-treated parental U2OS-HiLo cell lysates were used as a control. In order to identify co-precipitated proteins using a proteomics approach, HA immunoprecipitations were performed in triplicate, verified by immunoblot (Fig 1A), run on SDS-PAGE gels (Fig EV1C), and analyzed by mass spectrometry (Fig EV1D). To identify proteins that interact specifically with A3A, we utilized the Proteome Discoverer proteomics analysis platform. Enriched proteins were compared between HiLo cells induced to express A3A and parental HiLo cells (Fig 1A, Dataset EV1). We found substantial concordance among three replicates; 74% of proteins identified were enriched in A3A-expressing cells compared to parental HiLo cells in each replicate (Fig 1B). Using a stringent *P*-value cut-off of 0.05 (by one-tailed *t*-test) to define significance, we identified 63 proteins that were significantly enriched by affinity purification from A3A-expressing U2OS cells as compared to doxycycline-treated parental cells (Dataset EV1). We used the STRING database (Snel *et al*, 2000; Szklarczyk *et al*, 2019) to further investigate functional interactions among A3A co-precipitated proteins. Gene Ontology analysis of the proteins that were significantly enriched in the A3A dataset when compared to the parental dataset revealed all eight members of the CCT molecular chaperonin complex (CCT1-8) (Fig 1C and D). In addition, A3A immunoprecipitated with immune response proteins and ribonucleotide-binding proteins (Fig 1D). Given the striking enrichment of each CCT subunit among proteins that co-immunoprecipitated with A3A, we chose to further study the role of the CCT complex interaction with A3A (Fig 1C and D).

The CCT complex interacts specifically with A3A

To confirm the interaction between the CCT complex and A3A, we used a lentiviral expression system to engineer inducible A3A expression in two human cell lines (osteosarcoma U2OS cells and hepatic HepaRG cells) and evaluated co-immunoprecipitation with CCT subunits. First, we immunoprecipitated A3A-HA and used antibodies to CCT subunits to demonstrate CCT co-precipitation (Fig 2A). Next, in reciprocal experiments we immunoprecipitated the CCT complex using antibodies to endogenous CCT subunits and found that A3A was pulled down (Fig 2B). To address the interaction in physiologically relevant tissues, we engineered additional cell lines to express inducible A3A including hematopoietic cells (CEM, Ramos, K562) and breast cancer cells (MDA-MB-231). Expression and mutational activity of A3A has been previously demonstrated in both hematopoietic cancers and breast tumors (Nik-Zainal *et al*, 2012; Burns *et al*, 2013a; Green *et al*, 2017; Cortez *et al*, 2019; Jalili *et al*, 2020). We immunoprecipitated A3A from several leukemia cell lines and again found that the CCT complex was isolated (Fig 2C). In breast cancer cells, we performed reciprocal co-immunoprecipitations to demonstrate the A3A-CCT interaction (Fig 2D). These data validate the interaction between A3A and the CCT complex that we identified by proteomic analysis, including in tissues in which A3A has been shown to impact cancer genomes.

We then asked whether the CCT complex interacts with other APOBEC3 family members. The APOBEC3 proteins are highly

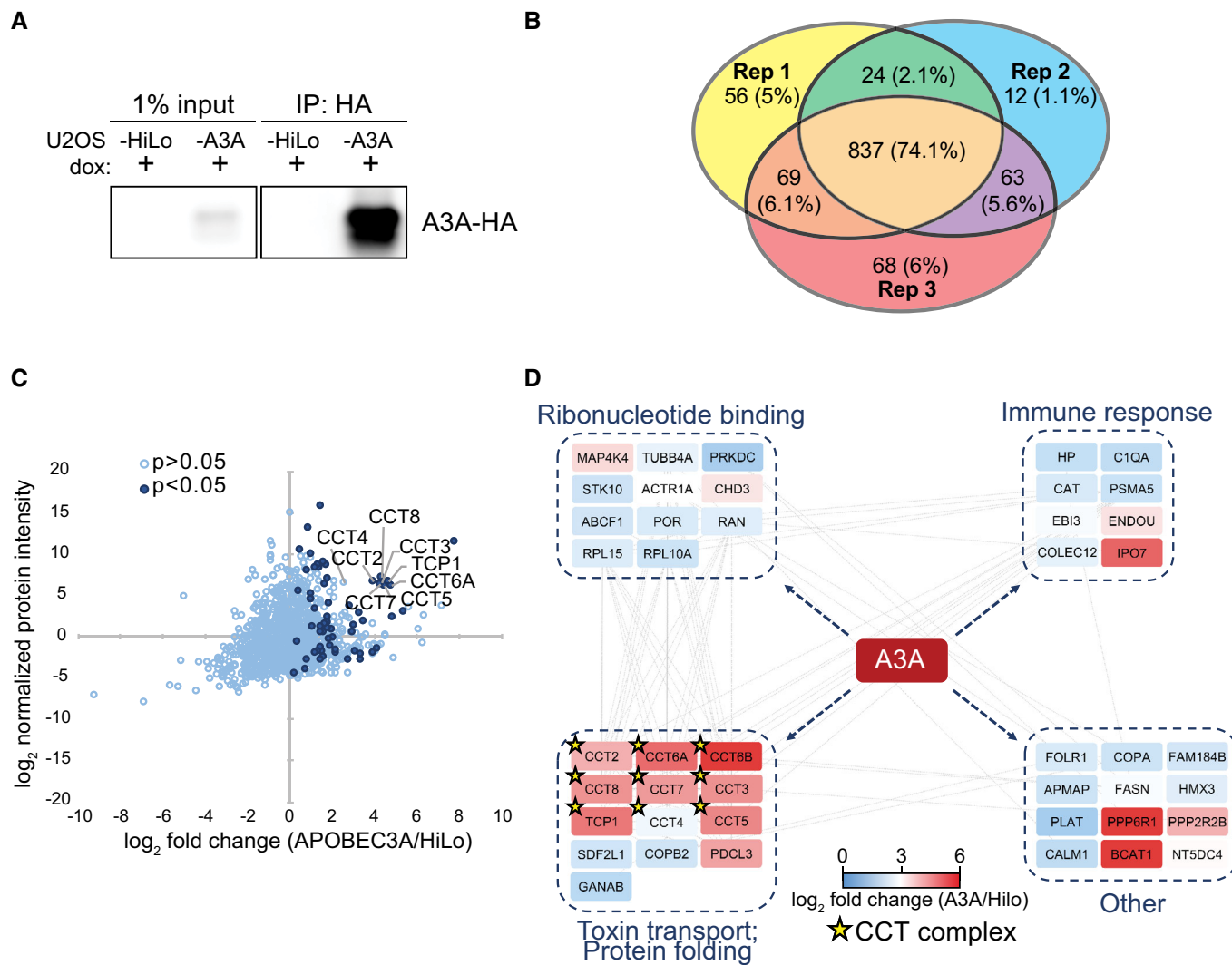


Figure 1. APOBEC3A interacts with all subunits of the CCT chaperonin complex.

A Immunoprecipitation of A3A. U2OS-HiLo cells with doxycycline-inducible, haemagglutinin (HA)-tagged A3A (U2OS-A3A) and parental cells (U2OS-HiLo without transgene) were treated with dox for 72 h. Immunoblot detection of A3A-HA after immunoprecipitation (IP) of cell lysates with anti-HA antibody is shown.

B Comparison of mass spectrometry results from three ($n = 3$) replicates. IP followed by mass spectrometry was performed in triplicate for parental U2OS-HiLo and U2OS-A3A cell lines. Venn diagram shows the overlap of proteins identified in three biological replicates of HA immunoprecipitation from U2OS-A3A cells. Number of proteins identified in each replicate is displayed along with the percentage of protein overlap identified between replicates.

C All eight subunits of the CCT chaperonin complex were enriched in U2OS-A3A samples. Proteins detected by MS are displayed by fold enrichment (\log_2) from U2OS-A3A cells compared to parental cells (x-axis) and by protein abundance within the U2OS-A3A samples (y-axis). Significantly enriched proteins ($P < 0.05$ by one-tailed t -test, $n = 3$) are denoted in dark blue. Components of the CCT complex are highlighted and labeled.

D Network of specific interactors of APOBEC3A. Only proteins significantly enriched in A3A samples over HiLo were considered for network analysis (\log_2 fold change > 0 ; one-tailed t -test $P < 0.05$), with the exception of CCT6B and CCT4 (t -test $P > 0.05$). Node colors denote enrichment (indicated by heatmap legend) of interacting protein in A3A samples compared to HiLo. Nodes are grouped into boxes according to gene ontology enriched biological processes for interacting proteins (STRING database, FDR < 0.01). Gray edge lines indicate observed interactions between proteins. CCT complex members are denoted by a star.

Source data are available online for this figure.

similar; the degree of homology between A3A and A3B or A3G is higher than 50% (Jarmuz *et al*, 2002; Narvaiza *et al*, 2009; Bulliard *et al*, 2011). Thus, we sought to determine whether homologous APOBEC3 enzymes also interact with CCT. Ectopic expression of HA-tagged A3A, A3B, and A3G was achieved by transfection of expression vectors into 293T cells. Immunoprecipitation of the CCT complex demonstrated co-precipitation with only A3A, and not A3B

or A3G (Fig 3A). The converse experiment, in which the APOBEC3 proteins were immunoprecipitated, revealed that only A3A pull-down resulted in co-precipitation of CCT complex subunits (Fig 3B). To ensure that this result was generalizable across cellular contexts, we immunoprecipitated doxycycline-inducible HA-tagged APOBEC3 proteins expressed in U2OS cell lines. We evaluated A3A and A3B and found that A3A, but not A3B, co-precipitated with the CCT

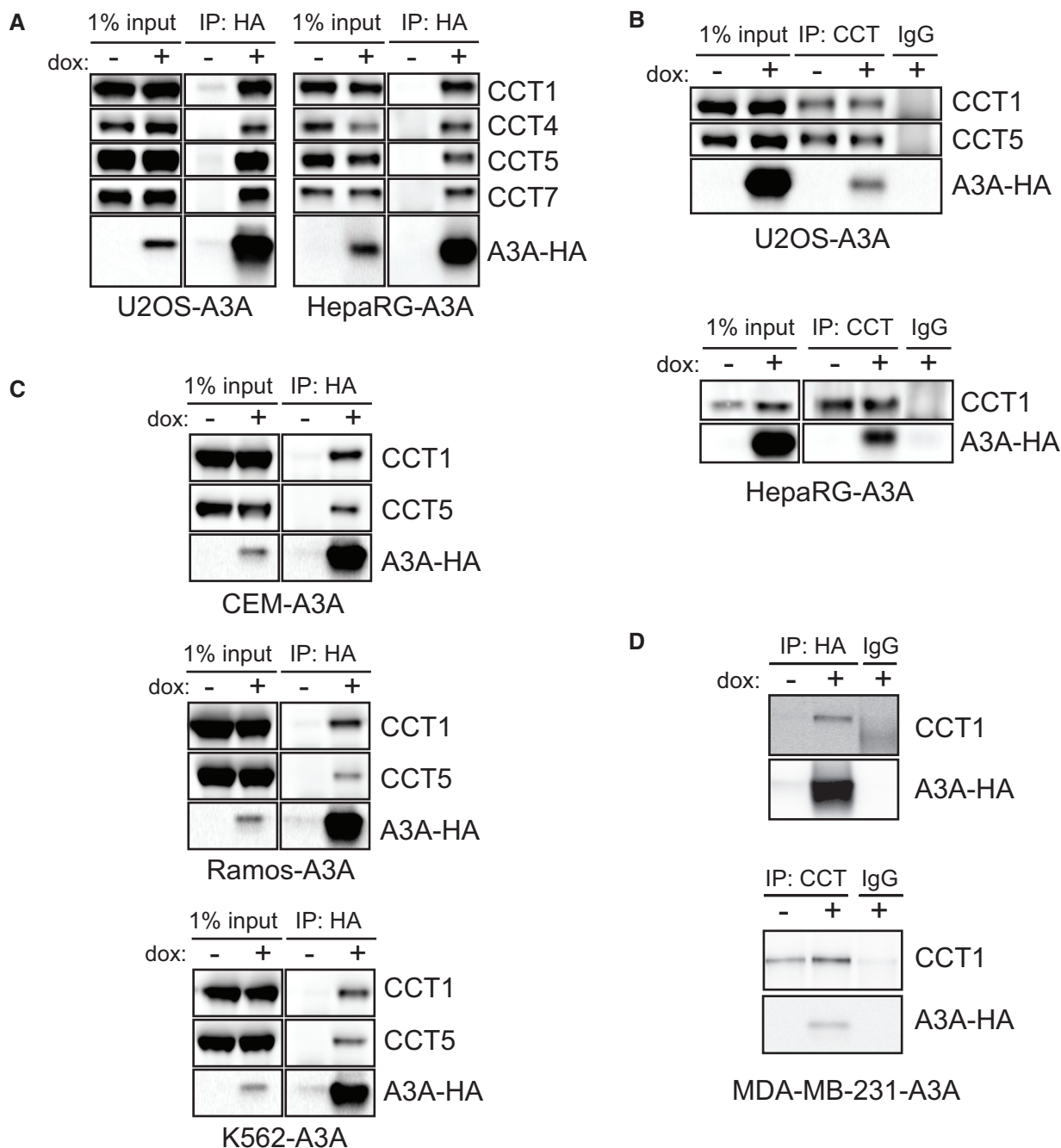


Figure 2. The CCT complex interacts with APOBEC3A in multiple cell types.

- A A3A co-precipitates with CCT complex subunits. U2OS and HepaRG cells with dox-inducible A3A-HA transgenes were treated with dox prior to immunoprecipitation of HA. HA immunoprecipitates were analyzed by immunoblot with antibodies for HA and subunits of the CCT complex.
- B Immunoprecipitation of CCT. IP of the CCT complex using antibodies to endogenous CCT subunits was performed in lysates from U2OS-A3A (top) and HepaRG-A3A (bottom) cells after dox treatment. Immunoblot analysis with probes for A3A-HA and indicated subunits of CCT with IgG as a control is shown.
- C A3A interacts with CCT in leukemia cells. HA immunoprecipitation in hematopoietic cell lines with inducible A3A-HA was analyzed by immunoblot. HA, CCT1, and CCT5 antibodies were used to evaluate co-precipitation of CCT subunits with A3A.
- D The CCT-A3A interaction occurs in breast cancer cells. HA (top) and CCT (bottom) immunoprecipitation in the MDA-MB-231 cell line with inducible A3A-HA expression was analyzed by immunoblot. Anti-HA and anti-CCT1 antibodies were used to evaluate reciprocal co-IPs.

Source data are available online for this figure.

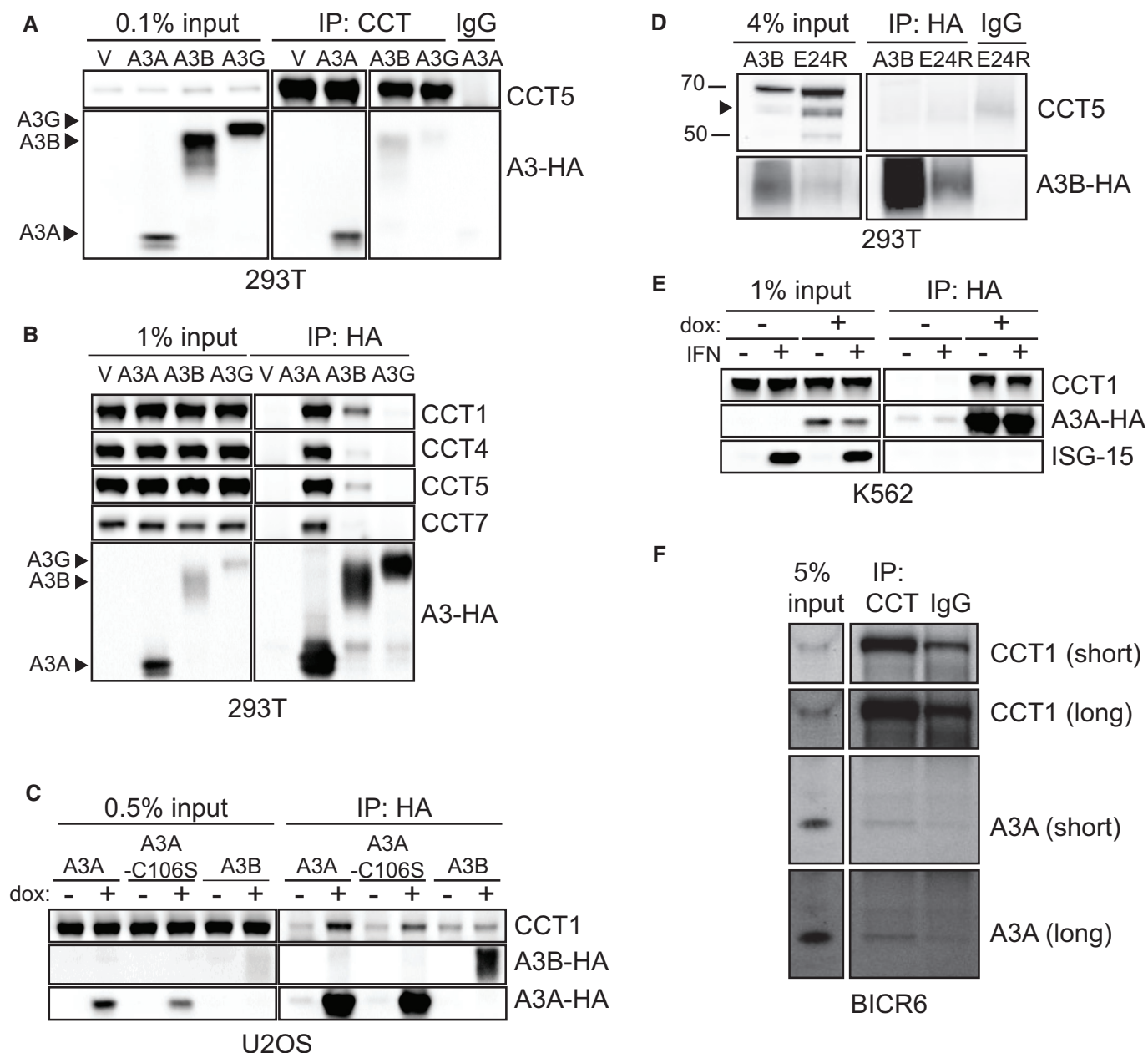


Figure 3. The APOBEC3-CCT interaction is specific to A3A.

A CCT co-precipitates with A3A but not A3B or A3G. 293T cells were transfected with empty vector (V), A3A-HA, A3B-HA, or A3G-HA. CCT IP was performed from transfected cells and evaluated by immunoblot analysis using antibodies for CCT5 and HA.

B A3A, but not other APOBEC3 enzymes, interacts with CCT complex subunits. After transfection of 293T cells with HA-tagged APOBEC3 expression plasmids, IP was performed with anti-HA antibody and analyzed by immunoblot using antibodies to HA and CCT subunits. Arrows mark location of each APOBEC3 protein on HA immunoblot.

C HA immunoprecipitation was performed from U2OS cells with dox-inducible A3A, A3A-C106S (catalytically inactive mutant), and A3B transgenes. IP lysates were evaluated by immunoblot using antibodies to HA and CCT1.

D Immunoprecipitation of HA-tagged A3B constructs transfected into 293T cells. IP of A3B-HA and A3B-E24R-HA (cytoplasmic localization) was evaluated by immunoblot analysis using antibodies to HA and CCT1. Arrow indicates CCT5 band.

E CCT interacts with A3A both with and without interferon. Immunoprecipitation of A3A-HA in K562 cells treated with and without type I interferon (IFN). Anti-ISG15 antibody serves as a control for IFN induction.

F CCT co-precipitates with endogenous A3A. Immunoprecipitation of the CCT complex in BICR6 cells was analyzed by immunoblot using antibodies to endogenous A3A and CCT1. Chemiluminescent exposure times described as short and long are indicated beside the blot. IgG antibody was used as a control throughout.

Source data are available online for this figure.

complex (Fig 3C). To determine whether catalytic activity of A3A is required for CCT binding, we performed immunoprecipitation of the catalytically inactive A3A-C106S mutant (Bogerd *et al*, 2006; Chen *et al*, 2006; Narvaiza *et al*, 2009). We found that the mutant co-precipitated with CCT subunits as efficiently as wild-type A3A (Fig 3C). Thus, a functional deaminase domain of A3A is not essential for CCT interaction. Our findings demonstrate that the APOBEC3-CCT interaction occurs specifically with A3A.

Since the subcellular localization of A3A differs from that of A3B, we asked whether cytosolic CCT required cytoplasmic localization of client APOBEC3 proteins for interaction. The A3B E24R mutant re-localizes nuclear A3B to the cytoplasm (Salamango *et al*, 2018). We immunoprecipitated wild-type A3B and A3B-E24R mutant and found that, although the A3B-E24R mutant appears to be less stable than wild-type A3B, neither co-precipitated with CCT complex subunits (Fig 3D). These data suggest that specificity of CCT interaction with A3A is not simply due to subcellular localization and may not be influenced by APOBEC3 amino acid sequence given the significant homology between A3A and other APOBEC3 proteins.

The A3A gene is interferon-stimulated and expression is increased significantly upon treatment with type I interferon (Chen *et al*, 2006; Koning *et al*, 2009). Although no prior reports have addressed the effect of interferon on CCT interaction with client proteins, we evaluated the impact on the A3A-CCT interaction. To accomplish this, we treated an interferon-responsive hematopoietic cell line, K562, with type I interferon. ISG-15, a canonical interferon-stimulated gene, was used as a control for interferon treatment. A3A was immunoprecipitated from cells treated with and without interferon, and there was no difference in CCT co-precipitation (Fig 3E). Thus, interferon does not appear to influence the interaction of A3A and CCT.

We addressed whether A3A and/or A3B, when endogenously expressed, interact with CCT. To do so, we utilized the BICR6 squamous cell carcinoma line in which A3A is expressed. Upon immunoprecipitation of the CCT complex, we found co-precipitation of A3A (Fig 3F). These data demonstrate that the A3A-CCT interaction occurs in the context of endogenous A3A expression.

Cytotoxicity from A3A is increased upon CCT depletion

Based on the specific and conserved interaction between A3A and CCT, we hypothesized that the CCT complex serves as a regulatory measure of the A3A protein. Since A3A can deaminate ssDNA at replication forks of cycling cells (Green *et al*, 2016; Hoopes *et al*, 2016; Seplyarskiy *et al*, 2016), we hypothesized that the CCT complex may prevent A3A from deaminating and damaging cellular DNA. To evaluate the impact of the A3A-CCT interaction on the genome, we investigated the outcome of disrupting the interaction by depleting CCT complex proteins. The CCT complex consists of stoichiometrically equal amounts of each protein, and free CCT complex subunits are rapidly degraded (Kunisawa & Shastri, 2003; Kasembeli *et al*, 2014). Consistent with previous reports (Kunisawa & Shastri, 2003; Kasembeli *et al*, 2014), we found that short interfering RNA (siRNA)-mediated knockdown of one CCT complex protein resulted in depletion of the remaining CCT complex members (Fig 4A), leading to effective suppression of CCT complex activities. We used siRNA to knock down CCT4 and CCT7 in U2OS cells,

which resulted in significant protein depletion (Fig 4B immunoblots). We evaluated the impact of A3A expression with CCT depletion in inducible cell lines and found that the combination of A3A expression and CCT depletion resulted in significantly decreased cell viability by WST-8 assay (Fig 4B bar graphs). We also evaluated cell death by live-dead staining in CCT-depleted cells and found a significant increase upon expression of A3A, greater than CCT depletion alone (Fig 4C). We hypothesized that the catalytic activity of A3A on the genome was responsible for increased genome instability resulting in cell death upon CCT depletion; thus, we evaluated the effect of a catalytically inactive A3A mutant (A3A-C106S) on cytotoxicity. Regardless of CCT depletion, we found no increase in cell death when the inactive A3A mutant was expressed (Fig 4D). Since A3A activity has been shown to cause DNA damage and elicit DNA damage response signaling including phosphorylation of histone variant H2AX (γ H2AX), a marker of DNA breaks (Landry *et al*, 2011; Burns *et al*, 2013a; Mussil *et al*, 2013; Green *et al*, 2016), we addressed whether A3A-mediated DNA damage was altered upon CCT depletion. To do so, CCT7 was depleted by siRNA targeting in K562 cells with ectopic inducible A3A expression. The combination of CCT7 depletion and A3A expression resulted in significantly increased γ H2AX as compared to controls (Fig 4E). Together, these data suggest that the interaction between CCT and A3A mitigates genome deamination, DNA damage, and genotoxicity.

A3A mutational signatures are enriched in cancers with deleterious CCT mutations

We next evaluated human tumors from The Cancer Genome Atlas (TCGA) to determine the effect of CCT depletion on A3A mutagenesis. APOBEC3 activity has been extrapolated from mutational patterns identified in cancer genome sequences, and the mutational hallmarks of A3A activity are thought to include a high burden of mutations with predominantly C→T transitions (Nik-Zainal *et al*, 2012; Alexandrov *et al*, 2013). We classified tumors with mutations within CCT genes that are predicted to cause negative effects on protein function, such as frameshift or non-sense mutations or indels, as having deleterious CCT gene mutations (Choi *et al*, 2012; McLaren *et al*, 2016). Tumors with deleterious mutations in one or more CCT complex proteins were compared to tumors with intact CCT genes (Fig 5). In total, 326 tumors had a deleterious mutation in one or more CCT genes as compared to 9,876 genomes with intact CCT complex genes. Mutations of individual CCT complex member genes were relatively evenly distributed in this data set, ranging from 8 to 20% of the 326 tumors identified with CCT complex mutations. We found that tumors with CCT gene mutations had a higher overall burden of mutations, and in particular C→T transitions, than those with intact CCT genes (Fig 5A). Mutational signatures, comprised of patterns of single base substitutions (SBS) identified within a trinucleotide context, have been used to determine mutagenic processes active in cancers (Alexandrov *et al*, 2020). Within the COSMIC database, mutational signatures attributed to APOBEC3 activity are denoted SBS2 and SBS13 (Alexandrov *et al*, 2020). Both signatures consist of predominantly cytidine mutations within a TC dinucleotide context, which is consistent with the context preference in which A3A deaminates cytidine bases (Chen *et al*, 2006). We evaluated the frequency of SBS2 and SBS13 in genomes from tumors with deleterious CCT gene mutations and

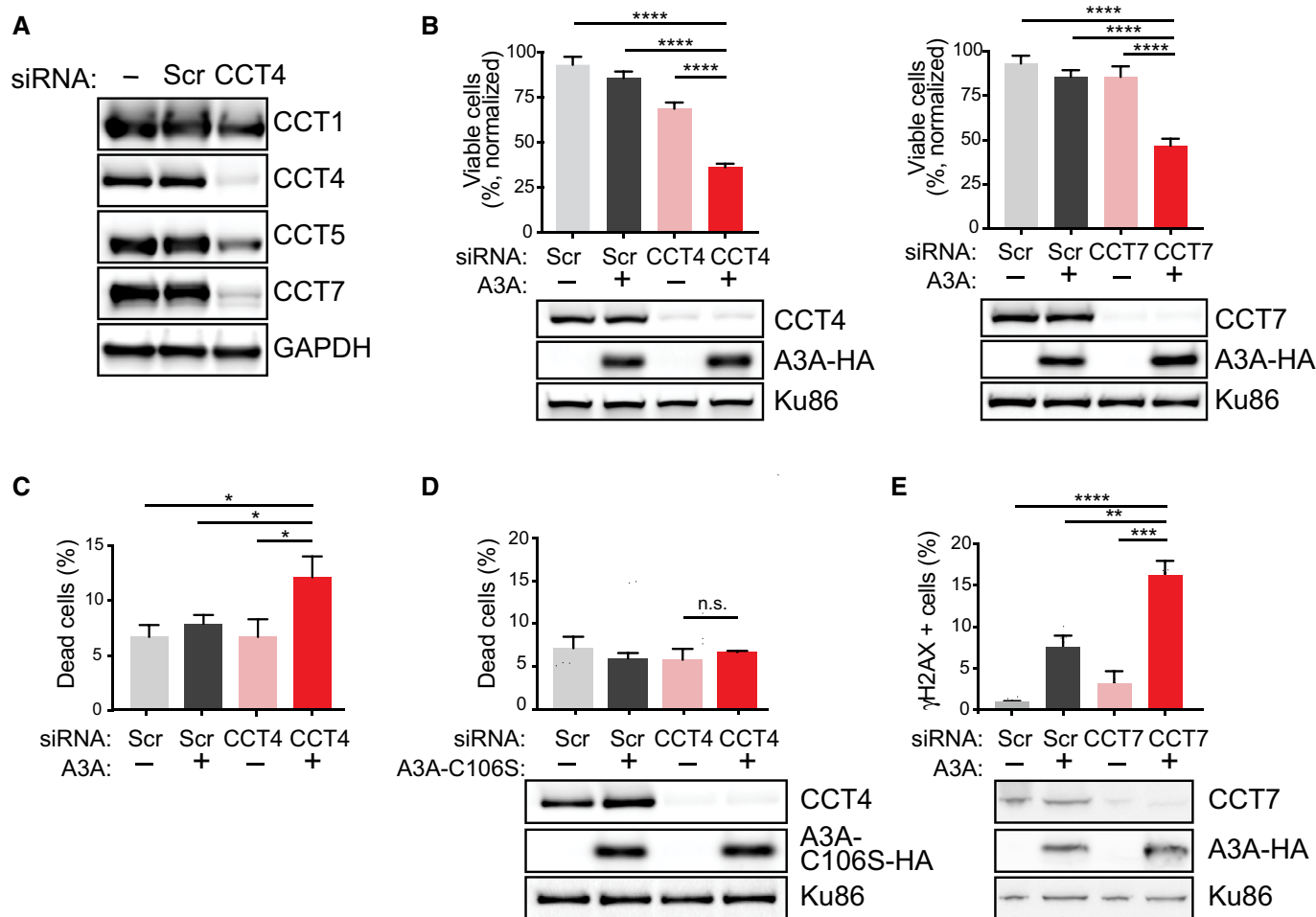


Figure 4. CCT complex depletion leads to decreased cell viability when A3A is expressed.

- A** Knockdown of one CCT complex member results in depletion of other CCT subunits. Following siCCT4 or siCCT7 transfection, cell lysates were evaluated by immunoblot for expression of additional CCT subunits by endogenous antibodies for CCT1, CCT4, CCT5, and CCT7. GAPDH was used as a loading control.
- B** Decreased cell viability upon CCT depletion and A3A expression. CCT4 (left) and CCT7 (right) subunits were depleted by siRNA transfection in U2OS cells with dox-inducible A3A transgenes. Immunoblot analysis of cell lysates showed decreased expression of targeted CCT subunit, but no alteration in A3A expression. Scr indicates non-targeted siRNA, used as control. Ku86 is a loading control. Following siRNA transfection to deplete CCT subunits, U2OS-A3A cells were treated with dox. Viability was determined by colorimetric change after addition of a water-soluble tetrazolium salt. Percent viability was normalized to untreated controls. Statistical analysis was performed using a paired two-tailed *t*-test, *n* = 3 biological replicates; error bars, SEM.
- C** Increased cell death resulting from A3A expression along with depletion of CCT. U2OS-A3A cells were depleted of CCT4 by siRNA, treated with dox, or combination. Cell death was measured by staining cells with fluorescent-labeled calcein AM (live) and DNA (dead) stains. Bar chart shows quantitation of FACS results averaged over three biological replicates. Statistical analysis was performed using a paired two-tailed *t*-test, *n* = 3; error bars, SEM.
- D** Viability of cells with catalytically inactive A3A. U2OS-A3A-C106S cells were induced with dox to express the catalytically inactive A3A mutant (C106S), depleted of CCT4 by siRNA, or combination. Cells were subsequently evaluated by live-dead staining assessed by FACS. Bar chart shows quantitation of FACS results averaged over three biological replicates. Statistical analysis was performed using a paired two-tailed *t*-test, *n* = 3; error bars, SEM. Immunoblot analysis of cell lysates showed decreased expression of CCT4 after siRNA targeting. Ku86 is a loading control.
- E** Increased DNA damage signaling upon CCT depletion and A3A expression. Depletion of CCT7 in K562-A3A cells was achieved by siRNA targeting. Expression of A3A was induced by dox treatment. Intracellular staining with anti- γ H2AX antibody was analyzed by flow cytometry. Bar chart shows quantitation of FACS results obtained over three biological replicates. Statistical analysis was performed using a two-tailed *t*-test, *n* = 3; error bars, SEM. Immunoblot analysis of cell lysates showed decreased expression of CCT7 after siRNA targeting and A3A expression upon dox treatment. Ku86 is a loading control. ***P*-value < 0.01, ****P*-value < 0.001, *****P*-value < 0.0001, and n.s. non-significant.

Source data are available online for this figure.

found a significant increase in both SBS2 and SBS13 as compared to tumors with intact CCT genes (Fig 5B). As a control, we performed a parallel evaluation of tumors with deleterious mutations in a randomly chosen set of nine genes which were of similar size to the CCT complex genes and were mutated with similar frequency to the

CCT complex genes (Fig EV2). Although the random gene set-mutated tumors harbored mutational burdens similar to CCT-mutated tumors (Fig EV2A), we found that the increase in SBS2 and SBS13 occurred more so in the CCT-mutated tumors (though not significant for SBS2, Fig EV2B). Thus, it appears that the mutational

pattern of APOBEC3 activity is enriched more so in cancer genomes from tumors with dysfunctional CCT complexes.

Next, we addressed mutational signatures in a subset of tumors in which APOBEC3 activity or expression has been specifically reported including breast, cervical, and bladder cancer (Nik-Zainal *et al*, 2012; Burns *et al*, 2013a; Faltas *et al*, 2016; Robertson *et al*,

2017). APOBEC3 mutational signatures SBS2 and SBS13 were quantified in the aforementioned tumors from TCGA (Fig 5C). In all tissue types, the APOBEC3 signatures were increased in tumors with CCT gene mutations compared to those with intact CCT genes. Finally, the contribution of all COSMIC SBS signatures to total mutation burden was assessed in TCGA samples. The contribution of SBS2

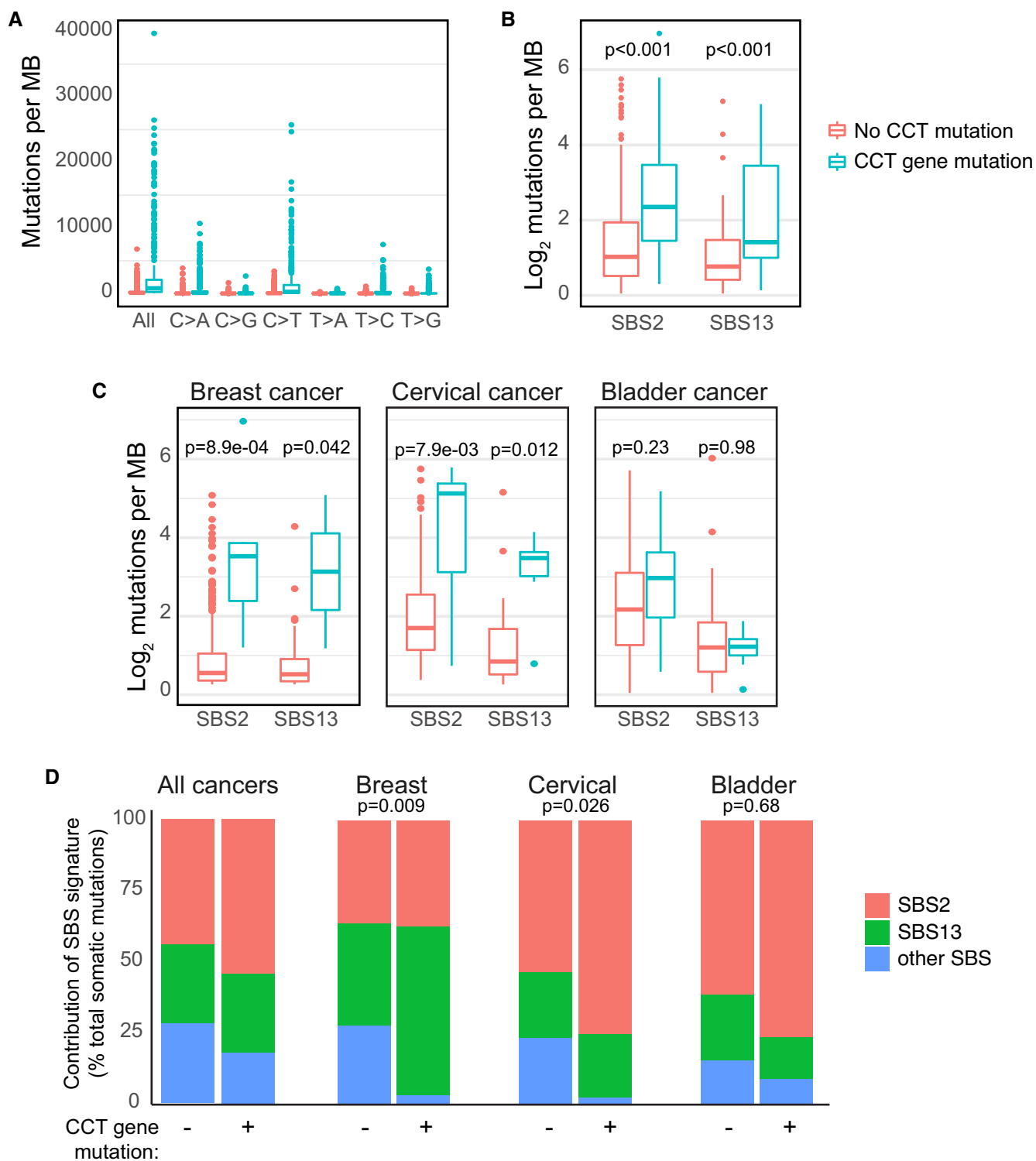


Figure 5.

Figure 5. A3A mutational signatures are enriched in cancers with CCT mutations.

- A Tumors with CCT gene mutations have an increased mutational burden. All cancer genome sequences in TCGA were evaluated for mutation burden and specific base substitutions. Cancers with CCT gene mutations predicted to cause a negative impact on protein function were classified as deleterious and were compared to those with no mutations in any CCT gene. Wilcoxon rank sum test applied to all paired comparisons between tumors with and without CCT gene mutations yielded $P < 0.001$.
- B The APOBEC3 mutational signature is enriched in tumors with CCT gene mutations. Single base substitution (SBS) patterns, as defined by COSMIC Mutational Signatures v2, were evaluated in CCT-mutated and CCT non-mutated cancer genome sequences. Depicted are the mutational signatures attributable to APOBEC3 activity (SBS2 and SBS13). Denoted P -values determined by Wilcoxon rank sum test.
- C Quantification of APOBEC3 mutational signatures among three tumor types that have previously been associated with high APOBEC3 activity. Breast, bladder, and cervical cancer samples from the TCGA database were divided into CCT-mutated and non-mutated genomes, as above. The number of mutations contributing to SBS2 and SBS13 in each tumor type was quantified and displayed as an average. Comparison by Wilcoxon rank sum test yielded P -values denoted.
- D The contribution of APOBEC3 mutational signatures (SBS2 and SBS13) and all other SBS signatures defined by COSMIC v2 was evaluated in all tumors and independently in breast, bladder, and cervical cancer genomes within the TCGA database. A comparison of mutational signature contributions between CCT-mutated and non-mutated tumors is shown. A z-test of proportions was used to compare whether the percentage of "other" signatures is significantly different between CCT-mutated and non-mutated tumors, and P -values show statistical significance in breast and cervical cancers but not in bladder cancer.

Data information: Box and whisker plots depict median and interquartile range (25–75%).

and SBS13 was higher in tumors which had CCT gene mutations (Fig 5D). Of note, the combined contribution of all other SBS signatures was lower in tumors with CCT gene mutations (Fig 5D), which suggests that APOBEC3 deamination is a predominant mutagenic process. We independently evaluated breast, cervical, and bladder tumors with and without CCT gene mutations and found an increased contribution of APOBEC3-associated SBS2 and SBS13 in tumors with CCT gene mutations as compared to tissue-matched controls with intact CCT genes (Fig 5D). When SBS2 and SBS13 were evaluated in control tumors with mutations in a random gene set, we found no increase in breast cancer genomes and a modest increase in cervical cancer genomes which was lower than the SBS2/13 mutations in CCT-mutated tumors (Fig EV2C and D). In bladder cancers, the contribution of SBS2 and SBS13 was similar in control tumors and those with CCT gene mutations (Fig EV2D). Taken together, these findings suggest overall that CCT dysfunction in human tumors is associated with increased APOBEC3 activity on the genome.

The role of APOBEC3 enzymes in cancer mutagenesis remains enigmatic, in part because our mechanistic understanding of these endogenous DNA mutators in relation to the host genome is incomplete. The two main bodies of evidence that link APOBEC3 enzymes to cancer indicate that (i) APOBEC3 enzymes are expressed at abnormally high levels in a subset of human cancers and (ii) a mutational pattern consistent with APOBEC3 deaminase activity is widespread in cancer genome sequences. However, correlation between APOBEC3 expression and activity has been weak at best, both experimentally and in primary tumor samples (Burns *et al*, 2013b; Chan *et al*, 2015; Cortez *et al*, 2019). In other words, the majority of cancer genome sequences which display APOBEC3 mutational hallmarks do not have elevated APOBEC3 expression levels (Petljak *et al*, 2019). This discord has been explained by hypothetical transient expression of APOBEC3 proteins which, upon genotoxicity, become downregulated (Roberts & Gordenin, 2014). However, this hypothesis does not explain the converse discordance, i.e., when high APOBEC3 expression is found in a tumor, the APOBEC3 mutational signature is often not enriched in the corresponding genome (Roberts *et al*, 2013; Petljak *et al*, 2019). This observation suggests that regulatory measures within a cell could mitigate APOBEC3 activity on the genome despite high expression.

In this study, we sought to identify protein interactors that influence the activity of A3A on the cellular genome.

Immunoprecipitation of A3A followed by mass spectrometry unexpectedly demonstrated an interaction with all subunits of the CCT chaperonin complex. The CCT chaperonin interacts with up to 15% of all cytosolic proteins, including an array of highly varied clients (Yam *et al*, 2008). The canonical client proteins of CCT are large and complex and include beta-rich strands and/or WD repeats (Thulasiraman *et al*, 1999; Kubota *et al*, 2006; Yam *et al*, 2008; Freund *et al*, 2014; Miyata *et al*, 2014). While A3A is not large, it has the classical structure of a DNA cytidine deaminase consisting of a fold composed of 5 beta-strands, 6 alpha-helices, and a zinc-coordinated domain (Byeon *et al*, 2013; Bohn *et al*, 2015). Thus, A3A shares some features with typical CCT client proteins.

The A3A-CCT interaction was reproducible across many cellular contexts and appears to be specific to A3A since no interaction between CCT subunits and A3B or A3G was observed. This specificity is curious given the high degree of homology between A3A and the C-terminal domains of A3B (93%) and A3G (66%). CCT is primarily found in the cytoplasmic compartment and A3A is expressed in both nucleus and cytoplasm, suggesting the interaction likely occurs in the cytoplasm similar to most CCT client proteins (Thulasiraman *et al*, 1999). In contrast to A3A, the A3B protein is located exclusively in the nucleus, and therefore, the interaction with CCT may have been limited by disparate subcellular localization. However, we also could not detect interaction with CCT for cytoplasmic A3B. The A3B protein has a similar DNA cytidine deaminase fold to that of A3A (Byeon *et al*, 2016); thus, we suspect that factors exogenous to the protein structure confer the specificity of the A3A-CCT interaction, presenting an area for future study.

Few protein interactors of A3A have been identified to date. The TRIB3 pseudokinase was previously reported to interact with A3A (Aynaud *et al*, 2012), and the interaction was suggested to inhibit A3A deamination of nuclear DNA (Aynaud *et al*, 2012). Similarly, we found that depletion of CCT resulted in increased deaminase-dependent DNA damage and cytotoxicity induced by A3A, suggesting that the CCT complex serves as a negative regulator of A3A activity on the genome. It is possible that this occurs indirectly through, for example, CCT interaction with a protein client that mediates repair of A3A-induced DNA damage. However, given our finding of a physical interaction between A3A and the CCT complex, we favor the likelihood of a direct impact of CCT on the A3A protein. Most substrates are released from the CCT complex upon folding, but in

some cases, CCT can act as a holdase. For example, the von Hippel-Lindau (VHL) protein is retained by CCT until the VHL binding partner, elongin-BC, interacts with VHL and enables release from CCT (Feldman *et al*, 1999). Similarly, a recent study demonstrated that CCT functions as a holdase for the reovirus capsid protein $\sigma 3$ to prevent aggregation of the protein prior to assembly into functional oligomeric complexes (Knowlton *et al*, 2018). It is possible that the CCT complex similarly functions as a holdase for A3A, thereby preventing access to the genome to minimize deamination and mutation. Further studies are required to determine the mechanism by which interaction with CCT mitigates A3A-induced mutagenesis. If the CCT-A3A interaction functions to sequester A3A, the signal for release may be related to the anti-viral properties of A3A. A possible model for the CCT-A3A interaction is that, upon viral infection, A3A is released from the CCT holdase and is therefore allowed to act on viral genomes leading to deamination, genome degradation, and viral restriction. In this model, disruption of the A3A-CCT interaction would allow for A3A mutagenesis of the cellular genome. Although our study did not find that treatment with type I IFN changed the A3A-CCT interaction, we did not directly assess whether viral infection disrupted the protein interaction.

The APOBEC3 mutational signature is among the most prevalent pattern of somatic mutagenesis in all sequenced cancer genomes (Petljak & Alexandrov, 2016). Here, we demonstrate that the hallmarks of APOBEC3 mutagenesis are increased in tumors with silencing mutations in CCT subunit genes. This provides one of the first examples of a cellular context that alters APOBEC3-mediated genotoxicity. It was recently suggested that targeting CCT may present a therapeutic anti-viral opportunity, since CCT is required for folding and assembly of viral capsid proteins (Knowlton *et al*, 2018). Inhibition of CCT may also present an opportunity to enable mutagenesis and genotoxicity selectively in cancer cells with high levels of A3A expression.

Materials and Methods

Cell lines

All cell lines were purchased from ATCC and tested for mycoplasma contamination every 6 months during experimentation. 293T, MDA-MB-231, and U2OS cells were maintained in DMEM supplemented with penicillin and streptomycin (100 U/ml) and 10% tetracycline-free fetal bovine serum (TF-FBS). BICR6 cells were maintained in DMEM supplemented with penicillin and streptomycin (100 U/ml), 10% fetal bovine serum (FBS), and 0.4 mg/ml hydrocortisone. HepaRG cells were maintained in William's Medium E, supplemented with penicillin and streptomycin (100 U/ml), 10% TF-FBS, L-glutamine (2 mM), hydrocortisone (0.5 μ M), and insulin (5 μ g/ml). CEM, Ramos, and K562 cells were maintained in RPMI media supplemented with 10% TF-FBS, penicillin and streptomycin (100 U/ml), and L-glutamine (2 mM).

Inducible U2OS-A3A, U2OS-A3B, U2OS-A3AC106S, MDA-MB-231-A3A, HepaRG-A3A, CEM-A3A, Ramos-A3A, and K562-A3A cells were generated by lentiviral transduction using the pSLIK-A3A lentivector with neomycin resistance, as previously described (Green *et al*, 2017). Inducible U2OS HiLo A3A cells were constructed by transfection of parental U2OS HiLo acceptor cells

with inducible plasmid cassette containing HA-tagged A3A along with plasmid expressing Cre recombinase, as previously described (Khandelia *et al*, 2011; Avgousti *et al*, 2016). All cells were induced by culture in the presence of doxycycline (0.1–5 μ g/ml). All cells were grown at 37°C under 5% atmospheric CO₂.

Antibodies

Commercially available antibodies used for immunoblotting, immunofluorescence, and intracellular staining were obtained from Abnova (CCT1, CCT5, CCT7), Santa Cruz Biotechnology (CCT4, ISG-15, Ku86, Tubulin), GeneTex (GAPDH), BD Biosciences (γ H2AX-488), BioLegend (HA), Cell Signaling (HA), and the NIH AIDS Reagent Program (APOBEC3A/G). Secondary antibodies for immunoblotting included goat anti-rabbit IgG and goat anti-mouse IgG (Jackson ImmunoResearch). Secondary antibodies for immunofluorescence included anti-Rabbit IgG (H + L), Alexa Fluor 488 (Invitrogen). For CCT immunoprecipitation, 1 μ g of each antibody was conjugated to protein G beads (Bio-Rad): CCT1 clone 2B2-D6 (Abnova), CCT4 clone H-1 (Santa Cruz), CCT5 clone 4E5-4B1 (Abnova), and CCT7 clone 1D6 (Abnova).

Plasmids, siRNA, and transfection

Expression vectors containing wild-type and mutant APOBEC3 cDNA with C-terminal HA epitopes have been previously described (Chen *et al*, 2006; Landry *et al*, 2011). Transfection of expression vectors was performed using Lipofectamine 2000 (Invitrogen) according to the manufacturer's protocol. Short interfering RNA (siRNA) targeting the CCT complex subunits was purchased from the Mission siRNA library (Sigma). Transfection of siRNA was achieved using the RNAiMAX transfection reagent (Invitrogen) according to the manufacturer's protocol.

Immunoblotting, immunofluorescence, and intracellular staining

For immunoblotting, lysates were harvested by boiling for 15 min at 95°C in 10% LDS sample buffer (Invitrogen) and 5% B-Mercaptoethanol (Sigma). Samples were run on Bis-Tris gels and transferred to nitrocellulose membrane (Amersham). For immunofluorescence, cells were fixed with 4% paraformaldehyde (15 min) and permeabilized with 0.5% Triton-X (10 min). Nuclei were visualized by 4,6-diamidino-2-phenylindole (DAPI, Sigma). Images were acquired by confocal microscopy. For intracellular antibody staining of γ H2AX, cells were harvested, fixed, and stained using the BD Cytofix/Cytoperm Kit according to the manufacturer's protocol. Events were acquired using an LSRFortessa flow cytometer (BD Biosciences) and analyzed by FlowJo (version 10.7).

HA immunoprecipitation

Cells were harvested in RIPA buffer, lysed on ice for 10 min, sonicated for 5 min at 4°C in Bioruptor (Diagenode UCD-200), and centrifuged to clear debris (25,000 g, 10 min, 4°C). Normalized lysates (1–3 mg total protein per 1 ml) were incubated with protein G beads (Invitrogen or Bio-Rad) on rotator (30 min, 4°C) and then incubated with Pierce™ Anti-HA Magnetic Beads (Thermo Scientific) on rotator (1–4 h, 4°C). Beads were washed three times in RIPA

buffer and eluted with LDS sample buffer (Invitrogen) by boiling (15 min, 95°C). For immunoblot analysis, 20% of eluate was run on NuPAGE™ 4–12% Bis-Tris Protein Gel (Invitrogen). For silver stain gel, 80% of eluate was run on NuPAGE™ 10% Bis-Tris Protein Gel (Invitrogen) and stained using the Silver Stain kit (Pierce) according to the manufacturer's protocol.

CCT complex immunoprecipitation

Cells were fixed with 1% paraformaldehyde (20 min) and quenched with 1.25 M glycine. Fixed cells were lysed as above. Normalized lysates (1.0 mg total protein in 1 ml) were incubated with protein G beads (Invitrogen or Bio-Rad) on rotator (30 min, 4°C). Antibody-conjugated protein G beads were incubated with normalized cell lysate on rotator (4 h, 4°C) and then washed and eluted as above. For experiments performed in BICR6 cells, fixation was not performed prior to immunoprecipitation. Lysates were prepared, normalized, cleared as above, and then incubated with antibody overnight (4°C) prior to 1-h incubation with protein G beads. Beads were then washed and protein was eluted as above.

Cell proliferation and viability assays

U2OS cells were transfected with siRNA for 72 h prior to evaluation. For proliferation assays, cells were seeded in 96-well plates, and water-soluble CCK-8 reagent (Dojindo) was added 2–4 h prior to analysis. Data were collected using the Infinity M1000 Pro plate reader (Tecan). To evaluate viability, cells were stained using the Live/Dead kit (Invitrogen) according to the manufacturer's instructions. Data were collected using an Accuri C6 Flow Cytometer (BD Biosciences).

Sample preparation for proteomic analysis

All chemicals used for preparation of nanoflow liquid chromatography–tandem mass spectrometry (nLC-MS/MS) samples were sequencing grade (Sigma-Aldrich), unless otherwise stated. The immunoprecipitation eluate (80–100%) was separated by SDS–PAGE using NuPAGE 1DE System (NuPAGE Novex 10% Bis-Tris gels, Thermo Fisher Scientific). Visualization of separated proteins was performed by overnight staining with Coomassie blue G-250 solution (Thermo Fisher Scientific). The in-gel tryptic digestion followed by peptide extraction from the gel bands was performed according to previously published protocols (Shevchenko *et al*, 1996). The extracted peptides were desalted using Poros Oligo R3 RP (PerSeptive Biosystems) P200 columns with C18 3M plug (3M Bioanalytical Technologies) prior to nLC–MS/MS analysis.

Nanoflow liquid chromatography–tandem mass spectrometry (nLC–MS/MS)

The peptide mixture was resuspended in buffer containing 0.1% formic acid and loaded onto an Easy-nLC system (Thermo Fisher Scientific), coupled online with an Orbitrap Fusion Tribrid mass spectrometer (Thermo Fisher Scientific). Peptides were loaded into a picofrit 18 cm long fused silica capillary column (75 µm i.d., 360 µm o.d.) packed in-house with reversed-phase ReproSil-Pur C18-AQ 3 µm resin. The gradient length was 75 min. The gradient

was from 2–26% buffer containing 100% ACN/0.1% formic acid at a flow rate of 300 nl/min. The MS method was set up in a data-dependent acquisition (DDA) mode. For full MS scan, the mass range of 350–1200 m/z was analyzed in the Orbitrap at 120,000 FWHM (200 m/z) resolution and 5×10^5 AGC target value. HCD collision energy was set to 27, AGC target to 10^4 , and maximum injection time to 120 ms. Detection of MS/MS fragment ions was performed in the ion trap in the rapid mode using the TopSpeed mode (3 s).

Protein identification and quantification

The raw mass spectrometer files were processed for protein identification using the Proteome Discoverer (v2.3, Thermo Scientific) and the Sequest HT algorithm with a peptide mass tolerance of 10 ppm, fragment m/z tolerance of 0.25 Da, and a false discovery rate (FDR) of 1% for proteins and peptides. All peak lists were searched against the UniProtKB/Swiss-Prot database of Human (March 2019, 20417 entries) sequences using the parameters as follows: enzyme, trypsin; maximum missed cleavages, 2; fixed modification, carbamidomethylation (C); variable modifications, oxidation (M), protein N-terminus acetylation. Protein quantifications were log₂-transformed and normalized using the median of the distribution for each sample. Every MS analysis was performed with three biological replicates to provide enough statistical power to apply parametric tests (either homoscedastic or heteroscedastic one-tailed *t*-test, depending on the statistical value of the *F*-test; heteroscedastic if *F*-test *P*-value < 0.05). The *t*-test was considered as a valuable statistical test because binary comparisons were performed, and the number of replicates was limited. No samples were excluded as outliers. Proteins with a *t*-test *P*-value < 0.05 were considered as significantly altered between the two tested conditions. Data distribution was assumed to be normal, but this was not formally tested. Gene Ontology (GO) biological process and protein–protein interaction information were obtained from STRING database (Snel *et al*, 2000; Szklarczyk *et al*, 2019) with false discovery rate (FDR) < 0.01.

Bioinformatic analysis

Single base substitutions (SBSs) and mutational signature information for TCGA tumors were obtained from the COSMIC database at <https://cancer.sanger.ac.uk/cosmic/signatures> (v2). Mutation calls made for the CCT complex genes were downloaded from the Genomic Data Commons Data Portal at <https://docs.gdc.cancer.gov/> (v22.0; Grossman *et al*, 2016). The data from these two databases were merged, and only tumors with one or more deleterious mutations in the CCT complex genes or tumors with intact CCT genes were kept for further analysis. All samples were subdivided by tumor type and mutation status of all CCT complex members. A tumor was considered wild-type when there were no single nucleotide variant or indels in any of the CCT complex genes, while mutations predicted by Ensembl VEP (McLaren *et al*, 2016) and SIFT (Choi *et al*, 2012) to cause a negative effect on protein function including indels, substitutions, frameshifts, and non-sense mutations were classified as deleterious. Additionally, tumors with non-deleterious mutations in the CCT complex genes as well as tumors without any somatic substitutions per megabase pairs were excluded for clarity of analysis. A control set of tumors was defined

by random selection of nine genes (CPNE1, RAD51B, NMUR2, KRT32, ALO24498.2, CFAP52, RSPH6A, PLSCR3, and SERPINB7) of analogous size to CCT complex genes and with similar mutation frequency (293 tumors with deleterious mutations in the random gene set compared to 9557 tumors without). Analysis of mutations and APOBEC enrichment between samples was computed and visualized using the R libraries ggplot2, dplyr, and tidyr, as well as a two-sided Mann–Whitney test to assess statistical significance.

Statistical analysis

Statistical details are reported in each figure legend. Each statistical analysis was performed on at least three biological replicates. The *t*-test was utilized for binary comparison of limited replicates. Analysis resulting in a *P*-value < 0.05 was considered to be significant.

Data availability

The datasets produced in this study are available in the following databases: Mass spectrometry proteomics data have been deposited to ProteomeXchange Consortium (<http://proteomecentral.proteomeexchange.org>) via the PRIDE partner repository (Perez-Riverol *et al*, 2019) with the dataset identifier PXD024191 or at <https://www.ebi.ac.uk/pride/archive/projects/PXD024191>.

Expanded View for this article is available online.

Acknowledgements

We thank all members of the Green and Weitzman laboratories for critical evaluation of experimental data and thoughtful review of the manuscript. We are thankful to our colleagues and collaborators for experimental discussions and manuscript review, in particular Dr. Daphne Avgousti, Dr. Nima Mosammaparast, and Dr. Nathan Singh. The results contained in this manuscript are in part based upon data generated by the TCGA Research Network: <https://www.cancer.gov/tcga>. This work was supported by a Young Investigator Award from the Alex's Lemonade Stand Foundation (AMG), K08 CA212299 (AMG), R01 CA181359 (MDW), R21 CA185799 (MDW), P01 CA196539 (BAG), and R01 AI118891 (BAG) from the National Institutes of Health, and support from the Children's Discovery Institute and the Washington University School of Medicine (AMG).

Author contributions

AMG and MDW conceived the project. RAD, DRO, ARH, KK, ASD, JHS, and KEH performed experiments. BAG supervised mass spectrometry and proteomics. AMG, RAD, DRO, KK, KEH, and MDW designed experiments and analyzed the data. AMG and MDW supervised the project, acquired funding, and wrote the manuscript.

Conflict of interest

The authors declare that they have no conflict of interest.

References

Alexandrov LB, Ju YS, Haase K, Van Loo P, Martincorena I, Nik-Zainal S, Totoki Y, Fujimoto A, Nakagawa H, Shibata T *et al* (2016) Mutational signatures associated with tobacco smoking in human cancer. *Science* 354: 618–622

Alexandrov LB, Kim J, Haradhvala NJ, Huang MN, Tian Ng AW, Wu Y, Boot A, Covington KR, Gordenin DA, Bergstrom EN *et al* (2020) The repertoire of mutational signatures in human cancer. *Nature* 578: 94–101

Alexandrov LB, Nik-Zainal S, Wedge DC, Aparicio SAJR, Behjati S, Biankin AV, Bignell GR, Bolli N, Borg A, Børresen-Dale A-L *et al* (2013) Signatures of mutational processes in human cancer. *Nature* 500: 415–421

Avgousti DC, Herrmann C, Kulej K, Pancholi NJ, Sekulic N, Petrescu J, Molden RC, Blumenthal D, Paris AJ, Reyes ED *et al* (2016) A core viral protein binds host nucleosomes to sequester immune danger signals. *Nature* 535: 173–177

Aynaud MM, Suspene R, Vidalain PO, Mussil B, Guetard D, Tangy F, Wain-Hobson S, Vartanian JP (2012) Human Tribbles 3 protects nuclear DNA from cytidine deamination by APOBEC3A. *J Biol Chem* 287: 39182–39192

Bogerd HP, Wiegand HL, Doehle BP, Lueders KK, Cullen BR (2006) APOBEC3A and APOBEC3B are potent inhibitors of LTR-retrotransposon function in human cells. *Nucleic Acids Res* 34: 89–95

Bohn MF, Shandilya SMD, Silvas TV, Nalivaika EA, Kouno T, Kelch BA, Ryder SP, Kurt-Yilmaz N, Somasundaran M, Schiffer CA (2015) The ssDNA Mutator APOBEC3A Is Regulated by Cooperative Dimerization. *Structure* 23: 903–911

Booth CR, Meyer AS, Cong Y, Topf M, Sali A, Ludtke SJ, Chiu W, Frydman J (2008) Mechanism of lid closure in the eukaryotic chaperonin Tric/CCT. *Nat Struct Mol Biol* 15: 746–753

Bulliard Y, Narvaiza I, Bertero A, Peddi S, Rohrig UF, Ortiz M, Zoete V, Castro-Diaz N, Turelli P, Telenti A *et al* (2011) Structure-function analyses point to a polynucleotide-accommodating groove essential for APOBEC3A restriction activities. *J Virol* 85: 1765–1776

Burns MB, Lackey L, Carpenter MA, Rathore A, Land AM, Leonard B, Refsland EW, Kotandeniya D, Tretyakova N, Nikas JB *et al* (2013a) APOBEC3B is an enzymatic source of mutation in breast cancer. *Nature* 494: 366–370

Burns MB, Temiz NA, Harris RS (2013b) Evidence for APOBEC3B mutagenesis in multiple human cancers. *Nat Genet* 45: 977–983

Byeon IJ, Ahn J, Mitra M, Byeon CH, Hercik K, Hritz J, Charlton LM, Levin JG, Gronenborn AM (2013) NMR structure of human restriction factor APOBEC3A reveals substrate binding and enzyme specificity. *Nat Commun* 4: 1890

Byeon IJ, Byeon CH, Wu T, Mitra M, Singer D, Levin JG, Gronenborn AM (2016) Nuclear magnetic resonance structure of the APOBEC3B catalytic domain: structural basis for substrate binding and DNA deaminase activity. *Biochemistry* 55: 2944–2959

Camasses A, Bogdanova A, Shevchenko A, Zachariae W (2003) The CCT chaperonin promotes activation of the anaphase-promoting complex through the generation of functional Cdc20. *Mol Cell* 12: 87–100

Cancer Genome Atlas Research Network, Albert Einstein College of Medicine, Analytical Biological Services, Barretos Cancer Hospital, Baylor College of Medicine, Beckman Research Institute of City of Hope, Buck Institute for Research on Aging, Canada's Michael Smith Genome Sciences Centre, Harvard Medical School, Helen F. Graham Cancer Center & Research Institute at Christiana Care Health Services *et al* (2017) Integrated genomic and molecular characterization of cervical cancer. *Nature* 543: 378–384

Chan K, Roberts SA, Klimczak LJ, Sterling JF, Saini N, Malc EP, Kim J, Kwiatkowski DJ, Fargo DC, Mieczkowski PA *et al* (2015) An APOBEC3A hypermutation signature is distinguishable from the signature of background mutagenesis by APOBEC3B in human cancers. *Nat Genet* 47: 1067–1072

Chen H, Lilley CE, Yu Q, Lee DV, Chou J, Narvaiza I, Landau NR, Weitzman MD (2006) APOBEC3A is a potent inhibitor of adeno-associated virus and retrotransposons. *Curr Biol* 16: 480–485

- Choi Y, Sims GE, Murphy S, Miller JR, Chan AP (2012) Predicting the functional effect of amino acid substitutions and indels. *PLoS One* 7: e46688
- Cong Y, Schröder GF, Meyer AS, Jakana J, Ma B, Dougherty MT, Schmid MF, Reissmann S, Levitt M, Ludtke SL et al (2012) Symmetry-free cryo-EM structures of the chaperonin TRiC along its ATPase-driven conformational cycle. *EMBO J* 31: 720–730
- Cortez LM, Brown AL, Dennis MA, Collins CD, Brown AJ, Mitchell D, Mertz TM, Roberts SA (2019) APOBEC3A is a prominent cytidine deaminase in breast cancer. *PLoS Genet* 15: e1008545
- Faltas BM, Prandi D, Tagawa ST, Molina AM, Nanus DM, Sternberg C, Rosenberg J, Mosquera JM, Robinson B, Elemento O et al (2016) Clonal evolution of chemotherapy-resistant urothelial carcinoma. *Nat Genet* 48: 1490–1499
- Feldman DE, Thulasiraman V, Ferreyra RG, Frydman J (1999) Formation of the VHL-elongin BC tumor suppressor complex is mediated by the chaperonin TRiC. *Mol Cell* 4: 1051–1061
- Freund A, Zhong FL, Venteicher AS, Meng Z, Veenstra TD, Frydman J, Artandi SE (2014) Proteostatic control of telomerase function through TRiC-mediated folding of TCAB1. *Cell* 159: 1389–1403
- Gao Y, Thomas JO, Chow RL, Lee GH, Cowan NJ (1992) A cytoplasmic chaperonin that catalyzes beta-actin folding. *Cell* 69: 1043–1050
- Gao Y, Vainberg IE, Chow RL, Cowan NJ (1993) Two cofactors and cytoplasmic chaperonin are required for the folding of alpha- and beta-tubulin. *Mol Cell Biol* 13: 2478–2485
- Green AM, Budagyan K, Hayer KE, Reed MA, Savani MR, Wertheim GB, Weitzman MD (2017) Cytosine deaminase APOBEC3A sensitizes leukemia cells to inhibition of the DNA replication checkpoint. *Cancer Res* 77: 4579–4588
- Green AM, Landry S, Budagyan K, Avgousti DC, Shalhout S, Bhagwat AS, Weitzman MD (2016) APOBEC3A damages the cellular genome during DNA replication. *Cell Cycle* 15: 998–1008
- Grossman RL, Heath AP, Ferretti V, Varmus HE, Lowy DR, Kibbe WA, Staudt LM (2016) Toward a shared vision for cancer genomic data. *N Engl J Med* 375: 1109–1112
- Harris RS, Dudley JP (2015) APOBECs and virus restriction. *Virology* 479–480: 131–145
- Hartl FU, Bracher A, Hayer-Hartl M (2011) Molecular chaperones in protein folding and proteostasis. *Nature* 475: 324–332
- Hoopes JJ, Cortez LM, Mertz TM, Malc EP, Mieczkowski PA, Roberts SA (2016) APOBEC3A and APOBEC3B preferentially deaminate the lagging strand template during DNA replication. *Cell Rep* 14: 1273–1282
- Jalili P, Bowen D, Langenbacher A, Park S, Aguirre K, Corcoran RB, Fleischman AG, Lawrence MS, Zou L, Buisson R (2020) Quantification of ongoing APOBEC3A activity in tumor cells by monitoring RNA editing at hotspots. *Nat Commun* 11: 2971
- Jarmuz A, Chester A, Bayliss J, Gisbourne J, Dunham I, Scott J, Navaratnam N (2002) An anthropoid-specific locus of orphan C to U RNA-editing enzymes on chromosome 22. *Genomics* 79: 285–296
- Jin M, Liu C, Han W, Cong Y (2019) TRiC/CCT chaperonin: structure and function. *Subcell Biochem* 93: 625–654
- Joachimski LA, Walzthoeni T, Liu CW, Aebersold R, Frydman J (2014) The structural basis of substrate recognition by the eukaryotic chaperonin TRiC/CCT. *Cell* 159: 1042–1055
- Kaisari S, Sitry-Shevah D, Miniowitz-Shemtov S, Teichner A, Hershko A (2017) Role of CCT chaperonin in the disassembly of mitotic checkpoint complexes. *Proc Natl Acad Sci U S A* 114: 956–961
- Kasembeli M, Lau WC, Roh SH, Eckols TK, Frydman J, Chiu W, Tweardy DJ (2014) Modulation of STAT3 folding and function by TRiC/CCT chaperonin. *PLoS Biol* 12: e1001844
- Khandelia P, Yap K, Makeyev EV (2011) Streamlined platform for short hairpin RNA interference and transgenesis in cultured mammalian cells. *Proc Natl Acad Sci U S A* 108: 12799–12804
- Kitamura A, Kubota H, Pack CG, Matsumoto G, Hirayama S, Takahashi Y, Kimura H, Kinjo M, Morimoto RI, Nagata K (2006) Cytosolic chaperonin prevents polyglutamine toxicity with altering the aggregation state. *Nat Cell Biol* 8: 1163–1170
- Knowlton JJ, Fernandez de Castro I, Ashbrook AW, Gestaut DR, Zamora PF, Bauer JA, Forrest JC, Frydman J, Risco C, Dermody TS (2018) The TRiC chaperonin controls reovirus replication through outer-capsid folding. *Nat Microbiol* 3: 481–493
- Koning FA, Newman EN, Kim EY, Kunstman KJ, Wolinsky SM, Malim MH (2009) Defining APOBEC3 expression patterns in human tissues and hematopoietic cell subsets. *J Virol* 83: 9474–9485
- Kubota S, Kubota H, Nagata K (2006) Cytosolic chaperonin protects folding intermediates of Gbeta from aggregation by recognizing hydrophobic beta-strands. *Proc Natl Acad Sci U S A* 103: 8360–8365
- Kunisawa J, Shastri N (2003) The group II chaperonin TRiC protects proteolytic intermediates from degradation in the MHC class I antigen processing pathway. *Mol Cell* 12: 565–576
- Lackey L, Demorest ZL, Land AM, Hultquist JF, Brown WL, Harris RS (2012) APOBEC3B and AID have similar nuclear import mechanisms. *J Mol Biol* 419: 301–314
- Lackey L, Law EK, Brown WL, Harris RS (2013) Subcellular localization of the APOBEC3 proteins during mitosis and implications for genomic DNA deamination. *Cell Cycle* 12: 762–772
- Landry S, Narvaiza I, Linfesty DC, Weitzman MD (2011) APOBEC3A can activate the DNA damage response and cause cell-cycle arrest. *EMBO Rep* 12: 444–450
- Liu X, Lin CY, Lei M, Yan S, Zhou T, Erikson RL (2005) CCT chaperonin complex is required for the biogenesis of functional Plk1. *Mol Cell Biol* 25: 4993–5010
- Lopez T, Dalton K, Frydman J (2015) The mechanism and function of group II chaperonins. *J Mol Biol* 427: 2919–2930
- Malim MH, Bieniasz PD (2012) HIV restriction factors and mechanisms of evasion. *Cold Spring Harb Perspect Med* 2: a006940
- McLaren W, Gil L, Hunt SE, Riat HS, Ritchie GR, Thormann A, Flicek P, Cunningham F (2016) The ensembl variant effect predictor. *Genome Biol* 17: 122
- Mitra M, Hercik K, Byeon I-J, Ahn J, Hill S, Hinchee-Rodriguez K, Singer D, Byeon C-H, Charlton LM, Nam G et al (2014) Structural determinants of human APOBEC3A enzymatic and nucleic acid binding properties. *Nucleic Acids Res* 42: 1095–1110
- Miyata Y, Shibata T, Aoshima M, Tsubata T, Nishida E (2014) The molecular chaperone TRiC/CCT binds to the Trp-Asp 40 (WD40) repeat protein WDR68 and promotes its folding, protein kinase DYRK1A binding, and nuclear accumulation. *J Biol Chem* 289: 33320–33332
- Mohanram V, Skold AE, Bachle SM, Pathak SK, Spetz AL (2013) IFN-alpha induces APOBEC3G, F, and A in immature dendritic cells and limits HIV-1 spread to CD4+ T cells. *J Immunol* 190: 3346–3353
- Mussil B, Suspene R, Aynaud MM, Gaurvit A, Vartanian JP, Wain-Hobson S (2013) Human APOBEC3A isoforms translocate to the nucleus and induce DNA double strand breaks leading to cell stress and death. *PLoS One* 8: e73641

- Narvaiza I, Linfesty DC, Greener BN, Hakata Y, Pintel DJ, Logue E, Landau NR, Weitzman MD (2009) Deaminase-independent inhibition of parvoviruses by the APOBEC3A cytidine deaminase. *PLoS Pathog* 5: e1000439
- Nik-Zainal S, Alexandrov L, Wedge D, Van Loo P, Greenman C, Raine K, Jones D, Hinton J, Marshall J, Stebbings L et al (2012) Mutational processes molding the genomes of 21 breast cancers. *Cell* 149: 979–993
- Ooms M, Krikoni A, Kress AK, Simon V, Munk C (2012) APOBEC3A, APOBEC3B, and APOBEC3H haplotype 2 restrict human T-lymphotropic virus type 1. *J Virol* 86: 6097–6108
- Peng G, Lei KJ, Jin W, Greenwell-Wild T, Wahl SM (2006) Induction of APOBEC3 family proteins, a defensive maneuver underlying interferon-induced anti-HIV-1 activity. *J Exp Med* 203: 41–46
- Perez-Riverol Y, Csordas A, Bai J, Bernal-Llinares M, Hewapathirana S, Kundu DJ, Inuganti A, Griss J, Mayer G, Eisenacher M et al (2019) The PRIDE database and related tools and resources in 2019: improving support for quantification data. *Nucleic Acids Res* 47: D442–D450
- Petljak M, Alexandrov LB (2016) Understanding mutagenesis through delineation of mutational signatures in human cancer. *Carcinogenesis* 37: 531–540
- Petljak M, Alexandrov LB, Brummel JS, Price S, Wedge DC, Grossmann S, Dawson KJ, Ju YS, Iorio F, Tubio JMC et al (2019) Characterizing mutational signatures in human cancer cell lines reveals episodic APOBEC mutagenesis. *Cell* 176: 1282–1294.e20
- Refsland EW, Stenglein MD, Shindo K, Albin JS, Brown WL, Harris RS (2010) Quantitative profiling of the full APOBEC3 mRNA repertoire in lymphocytes and tissues: implications for HIV-1 restriction. *Nucleic Acids Res* 38: 4274–4284
- Reissmann S, Joachimiak LA, Chen B, Meyer AS, Nguyen A, Frydman J (2012) A gradient of ATP affinities generates an asymmetric power stroke driving the chaperonin TRiC/CCT folding cycle. *Cell Rep* 2: 866–877
- Roberts SA, Gordenin DA (2014) Hypermutation in human cancer genomes: footprints and mechanisms. *Nat Rev Cancer* 14: 786–800
- Roberts SA, Lawrence MS, Klimczak LJ, Grimm SA, Fargo D, Stojanov P, Kiezun A, Kryukov GV, Carter SL, Saksena G et al (2013) An APOBEC cytidine deaminase mutagenesis pattern is widespread in human cancers. *Nat Genet* 45: 970–976
- Robertson AG, Kim J, Al-Ahmadie H, Bellmunt J, Guo G, Cherniack AD, Hinoue T, Laird PW, Hoadley KA, Akbani R et al (2017) Comprehensive molecular characterization of muscle-invasive bladder cancer. *Cell* 171: 540–556.e25
- Rommelaere H, Van Troys M, Gao Y, Melki R, Cowan NJ, Vandekerckhove J, Ampe C (1993) Eukaryotic cytosolic chaperonin contains t-complex polypeptide 1 and seven related subunits. *Proc Natl Acad Sci U S A* 90: 11975–11979
- Roper N, Gao S, Maity TK, Banday AR, Zhang Xu, Venugopalan A, Cultraro CM, Patidar R, Sindiri S, Brown A-L et al (2019) APOBEC mutagenesis and copy-number alterations are drivers of proteogenomic tumor evolution and heterogeneity in metastatic thoracic tumors. *Cell Rep* 26: 2651–2666.e6
- Salamango DJ, McCann JL, Demir O, Brown WL, Amaro RE, Harris RS (2018) APOBEC3B nuclear localization requires two distinct N-terminal domain surfaces. *J Mol Biol* 430: 2695–2708
- Seplyarskiy VB, Soldatov RA, Popadin KY, Antonarakis SE, Bazykin GA, Nikolaev SI (2016) APOBEC-induced mutations in human cancers are strongly enriched on the lagging DNA strand during replication. *Genome Res* 26: 174–182
- Shevchenko A, Wilm M, Vorm O, Mann M (1996) Mass spectrometric sequencing of proteins silver-stained polyacrylamide gels. *Anal Chem* 68: 850–858
- Snel B, Lehmann G, Bork P, Huynen MA (2000) STRING: a web-server to retrieve and display the repeatedly occurring neighbourhood of a gene. *Nucleic Acids Res* 28: 3442–3444
- Suspene R, Aynaud MM, Guetard D, Henry M, Eckhoff G, Marchio A, Pineau P, Dejean A, Vartanian JP, Wain-Hobson S (2011) Somatic hypermutation of human mitochondrial and nuclear DNA by APOBEC3 cytidine deaminases, a pathway for DNA catabolism. *Proc Natl Acad Sci U S A* 108: 4858–4863
- Szklarczyk D, Gable AL, Lyon D, Junge A, Wyder S, Huerta-Cepas J, Simonovic M, Doncheva NT, Morris JH, Bork P et al (2019) STRING v11: protein-protein association networks with increased coverage, supporting functional discovery in genome-wide experimental datasets. *Nucleic Acids Res* 47: D607–D613
- Tam S, Geller R, Spiess C, Frydman J (2006) The chaperonin TRiC controls polyglutamine aggregation and toxicity through subunit-specific interactions. *Nat Cell Biol* 8: 1155–1162
- Thulasiraman V, Yang CF, Frydman J (1999) *In vivo* newly translated polypeptides are sequestered in a protected folding environment. *EMBO J* 18: 85–95
- Trinidad AG, Muller PA, Cuellar J, Klejnot M, Nobis M, Valpuesta JM, Vousden KH (2013) Interaction of p53 with the CCT complex promotes protein folding and wild-type p53 activity. *Mol Cell* 50: 805–817
- Tyedmers J, Mogk A, Bukau B (2010) Cellular strategies for controlling protein aggregation. *Nat Rev Mol Cell Biol* 11: 777–788
- Vartanian JP, Guetard D, Henry M, Wain-Hobson S (2008) Evidence for editing of human papillomavirus DNA by APOBEC3 in benign and precancerous lesions. *Science* 320: 230–233
- Wang Z, Wakae K, Kitamura K, Aoyama S, Liu G, Koura M, Monjurul AM, Kukimoto I, Muramatsu M (2014) APOBEC3 deaminases induce hypermutation in human papillomavirus 16 DNA upon beta interferon stimulation. *J Virol* 88: 1308–1317
- Yam AY, Xia Y, Lin HT, Burlingame A, Gerstein M, Frydman J (2008) Defining the TRiC/CCT interactome links chaperonin function to stabilization of newly made proteins with complex topologies. *Nat Struct Mol Biol* 15: 1255–1262
- Yu Q, Konig R, Pillai S, Chiles K, Kearney M, Palmer S, Richman D, Coffin JM, Landau NR (2004) Single-strand specificity of APOBEC3G accounts for minus-strand deamination of the HIV genome. *Nat Struct Mol Biol* 11: 435–442